Jordan Journal of Civil Engineering, Volume **11**, No. **3**, **2017**

Size Effect on Fracture Properties of Self-Compacting Concrete Beams Using DIC Technique

Bhavin Patel [1)]***, Yogendra Tandel*** [2)]***, Atul Desai*** [3)] ***and Santosh Shah*** [4)]

[1)] S. V. National Institute of Technology, Surat, India. E-Mail: bhavinpatel2000@gmail.com
[2)] GIDC Degree, Engineering College, Navsari, India. E-Mail: ykt.ced@gdec.in
[3)] Professor, Applied Mechanics Department, S. V. National Institute of Technology, India. E-Mail: akd@amd.svnit.ac.in
[4)] Professor, Civil Eng. Dept., ITM Universe, India. E-Mail: santoshgshah@gmail.com

ABSTRACT

The main objective of this study is to develop a new measurement technique without touching the measured object. Digital Image Correlation (DIC) is an advanced measurement technique used to measure the displacement of particles with very high accuracy. This powerful innovative technique is used to correlate two image segments to determine the similarity between them. For this study, three geometrically similar beam specimens of different sizes were cast and tested under three-point bending in a closed loop servo-controlled machine with crack mouth opening displacement control with a rate of opening of 0.0005 mm/sec. Digital images were captured before loading (unreformed state) and at different instances of loading and analyzed using correlation techniques to compute surface displacement, crack opening and sliding displacement, load-point displacement, crack length and crack tip location. It was seen that crack mouth opening displacement and vertical load-point displacement computed using DIC analysis match well with those experimentally measured.

KEYWORDS: Self-compacting concrete, Experiments, Beam, Crack opening, Size effect, Digital image correlation.

INTRODUCTION

Self-compacting concrete (SCC) is a high-performance concrete that can flow under its own weight so as to completely fill the formwork and self-consolidate without any mechanical vibration (Erdem et al., 2009; Gaimster and Dixon, 2003). This type of concrete is specifically designed to achieve excellent deformability, low risk of blockage and good stability, ensuring a high formwork filling capacity. SCC is considered a suitable material for the construction of structural members with high volumes of steel reinforcement because of its ability to easily flow in highly congested areas (Najm, 2008; Skarendal, 2005).

Digital image correlation (DIC) has increasingly attracted attention in a variety of engineering areas, like experimental mechanics (Lava et al., 2009; Zhang et al., 2012; Chen et al., 2015; Wang and Ma, 2014), biomechanics (Huang, 2012; Zhang and Arola, 2004; Huang et al., 2010a; Huang et al., 2010b) and geophysics (Debella-Gilo and Kaab, 2011; Walter, 2011), owing to its well-known advantages in the aspect of full-field surface deformation measurements (Sutton et al., 2009; Wang et al., 2015; Zhu et al., 2015; Zhou et al., 2014; Wang et al., 2014; Dai et al., 2015). Electronic Speckle Photography (ESP) has been an active research

Received on 23/1/2017.
Accepted for Publication on 5/3/2017.

area since the past two decades, in which different parameters of the technique have been addressed for the improvement of accuracy in measurement results and for the removal of different defects encountered during experimentation. In ESP, two images-called reference (before the application of load) and test (after the application of load) images-of an optically rough surface under illumination by a light source (e.g. a laser beam) are recorded. These two speckle images are correlated using DIC for the measurement of in-plane displacements or deformations which the test image has undergone with respect to the reference image.

Considering the fact that the traditional DIC algorithm is usually so computationally intense that it is very difficult to meet some specified speed requirements for time critical applications or large-scale data processing tasks, on the other hand, some new numerical strategies, such as basis function and sum-table methods, have been developed to mathematically decrease the computational burden of DIC matching and hence increase the speed of integer-pixel correlation calculations to a great extent (Huang et al., 2010a; Huang et al., 2010b).

Objectives

The objectives of this study are:

- Development of self-compacting concrete.
- Monitoring of crack propagation using DIC technique.
- Measurement of beam deflection and crack width with the help of DIC technique.

Principles of DIC

Digital image correlation (DIC) is an optical, non-contact measurement technique adopted to analyze displacements on the surface of an object of interest. In digital image correlation, the surface images before and after deformation are taken by a digital camera from which the displacement at any point of the image is computed. DIC is extensively used to study a very large range of materials, in a widely different range of scales. It was originally developed in the 1980s (Sutton et al., 1983; Sutton et al., 1986). DIC-based methods and their fields of application have been steadily growing due to technological progress and affordability of digital imaging systems.

DIC is based on the following principles: the image of the body is described by a discrete function representing the grey level of each pixel. The grey level is a value between 0 and 255, with the lowest value representing black, the highest value representing white and values in between representing different shades of grey. The correlation calculations are carried out for a set of pixels, called a pattern. The displacement field is assumed to be homogeneous inside a pattern. The initial image representing the body before distortion is a discrete function f (x, y) and is transformed into another discrete function f^* (x^*, y^*) after distortion or displacement. The theoretical relation between the two discrete functions can be written as (Touchal et al., 1997):

$$f^*(x^*, y^*) - f(x + u(x,y), y + v(x,y)) = 0$$

where: u(x, y) and v(x, y) represent the displacement field for a pattern as shown in Figure. 1.

Image correlation now becomes a job of comparing sub-sets of numbers between the two digital images. A typical cross-correlation coefficient which measures how well sub-sets match is given by:

$$C = 1 - \frac{\sum[f(x,y).f^*(x^*,y^*)}{[\sum(f(x,y)^2).\sum f^*(x^*,y^*)^2]^{1/2}}$$

where: f (x, y) is the grey level value at coordinate (x, y) for the initial image and $f^*(x^*, y^*)$ is the grey level value at point (x^*, y^*) of the deformed image. The coordinates (x, y) and (x^*, y^*) are related by the deformation which has occurred between acquisition of the two images. If the motion of the object relative to the camera is parallel to the image plane, they are related by:

$$x^* = x + u + \frac{\partial \mathrm{u}}{\partial \mathrm{x}}\Delta x + \frac{\partial \mathrm{u}}{\partial \mathrm{y}}\Delta y$$

$$y^* = y + v + \frac{\partial \mathrm{v}}{\partial \mathrm{x}}\Delta x + \frac{\partial \mathrm{v}}{\partial \mathrm{y}}\Delta y$$

where: u and v are the displacements for the sub-set

centers in the x and y directions, respectively. The terms Δx and Δy are the distances from the sub-set center to point (x, y). By performing image correlation, the values of coordinates (x, y), displacement (u, v) and the derivatives of the displacements ∂u/∂x, ∂u/∂y, ∂v/∂x and ∂v/∂y can be determined (Touchal et al., 1997; Bruck et al., 1989). These are in turn used for further analysis, for example, in the computation of fracture parameters.

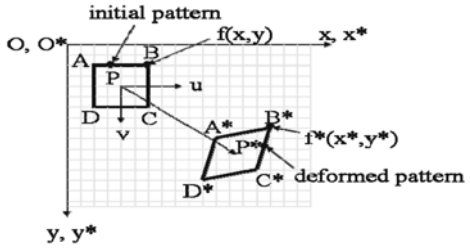

Figure (1): Initial and deformed patterns

EXPERIMENTAL RESEARCH

Materials

A list of materials used for this study is given along with their specifications in Table 1. The physical properties and particle size distribution of the sand and aggregates are given in Table 2.

Mix Proportions

To achieve self-capability, a number of trials were executed for different combinations of materials. Binder content varies between 450 kg/m^3 and 700 kg/m^3 and Water/Binder (W/B) ratio varies between 0.29 and 0.34 (by weight) with corresponding variation in the paste volume to investigate the influence of binder. The aggregate combination of 50:20:30 (fine aggregate: coarse aggregate of 10 mm maximum size: coarse aggregate of 20 mm maximum size) by volume was kept constant for all mixes.

A polycarboxylate-based high-range water reducing admixture (HRWRA) was also used in the mixtures; the dosage of superplasticizer was kept constant at 0.5% by weight of binder for providing the desired fluidity of the SCC. For all tests, the proportion of cement to fly ash was kept constant (cement: fly ash = 70:30). The constitution of each of the final mixes is presented in Table 3.

Table 1. Materials used in this study

Material	Specification
Ordinary Portland cement	As described in IS: 12269; specific gravity = 3.12
Fly ash	Dark, pozzocrete 60 conforming to IS: 3812 (Part 1) 2013; Specific gravity = 2.0
Superplasticizer	Master Glenium SKY 8276, BASF conforming to ASTM C 494
Fine aggregate	Locally available river sand passing through 4.75 mm IS sieve, conforming to IS: 3812 (Part 1) 2013
Coarse aggregate	Locally available crushed granite; maximum sizes of 20 mm and 10 mm, conforming to IS: 3812 (Part 1) 2013

Table 2. Physical properties of sand and aggregate

Properties	Sand	Coarse aggregate 10 mm maximum size	Coarse aggregate 20 mm maximum size
Specific gravity	2.62	2.8	2.78
Bulk density (loose, kg/m^3)	1708	1450	1414
Bulk density (compact, kg/m^3)	1868	1652	1632
Water absorption %	1.39	0.65	0.56

Table 3. Composition of reference mix

Constituent	Quantity (kg/m^3)
Cement	354
Fly ash	96
Fine aggregate	634
Coarse aggregate (<10 mm)	224
Coarse aggregate (<20mm)	332
Water	160*
Superplasticizer	2.225*

* in liters.

Specimen Preparation

The details of the specimen geometry and its nomenclature are shown in Figure 2 and Table 4, respectively. The concrete mixes are poured into their respective moulds of geometrically similar beams with three different sizes, each having a notch to depth ratio of 0.2 and a span to depth ratio of 2.5. In order to create a notch, a fine metal strip of 2 mm thickness was introduced during casting at the center for different notch sizes.

Table 4. Dimensions of beams

Parameters	Beam designation		
	Small	Medium	Large
Depth, d (mm)	76	152	304
Span, S (mm)	190	380	760
Length, L (mm)	241	431	810
Thickness, b (mm	50	50	50
Notch depth, a_0 (mm)	15.2	30.4	60.8

The rationale behind the selection of small, medium and large beams is to study the effect of specimen size on the fracture behavior by testing geometrically similar specimens as per the draft recommendation of the RILEM Technical Committee 89-FMT on fracture mechanics of concrete (RILEM, 1990). Using this method, one can obtain a size effect plot, by which the size of the structure can be extrapolated to a very large structure like a dam. The notch site is kept at the center of the beam under three-point bending as recommended by RILEM (1990). While handling the specimens, great care is taken to prevent any falling or impact on the specimens.

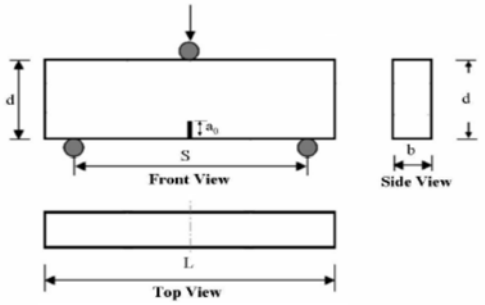

Figure (2): Details of the specimen geometry

Testing of Specimens

The specimens are tested in a closed loop servo-controlled testing machine having a capacity of 100 kN. A specially calibrated 50 kN load cell is used for measuring the load. The load-point displacement is measured using a linear variable displacement transformer (LVDT). The crack mouth opening displacement (CMOD) is measured using a clip gage located across the notch. All the tests are performed under CMOD control with the rate of crack opening being 0.0005 mm/s. The results of load, vertical displacement, CMOD and time are simultaneously acquired through a data acquisition system.

For digital image correlation, the speckle pattern is to be made on the specimen. The specimen is initially white washed and a speckle pattern is prepared over it using a standard black spray paint. The specimen images are captured before loading and during various stages of loading using a digital camera mounted on a stand. A remote control is used for capturing the images to avoid any vibration and also to keep the distance between camera lens and the specimen unchanged. Further, it is

known that a DIC measurement using a single camera introduces errors due to out-of-plane movements. Out-of-plane movements may result in losing some of the information of the image part under consideration. The bem specimens are tested under three-point bending and the supports as well as the loading cylinders are adjusted in such a way that the loading and reactions act in the plane of the specimen. Furthermore, the stiffness of the concrete specimens is relatively too large to cause any significant out-of-plane deformations. Hence, the out-of-plane movements are neglected in this work. It is assumed that a single image scale can be applied across the entire image to convert from image-space coordinates into object-space coordinates.

RESULTS AND DISCUSSION

Fresh Properties

Fresh properties of SCC are as important as its hardened properties. To evaluate workability of fresh self-compacting concrete, like filling ability, passing ability and segregation resistance, different tests were carried out as per EFNARC (2002) specifications. Filling ability of SCC was measured using slump flow and V – funnel tests. Passing ability of SCC was measured using J- ring, L- box and U – box tests. Similarly, resistance to segregation of self-compacting concrete was measured with the help of GTM screen stability test. All test results are presented in Table 5. Test results show that self-compacting concrete is satisfying all workability criteria specified by EFNARC.

Table 5. Fresh properties of self-compacting concrete

Workability Test	EFNARC Limit	Test Result
Slump Flow in mm	(650-800 mm)	760
T_{50} cm Slump Flow in Sec	(2-5 Sec)	4.2
J Ring	(H_1-H_2=0-10 mm)	6
J Ring Flow in mm	-	730
V-Funnel Flow in Sec	(6-12 Sec)	8
L-Box Blocking Ratio	(H_2/H_1=0.8-1.0)	0.93
U-Box Filling Height	(H_1-H_2=0-30 mm)	20

Mechanical Properties

After testing for fresh properties, concrete was filled in cubes, cylinder and beam moulds for mechanical properties. Concrete cubes of 150 mm × 150 mm × 150 mm dimensions were cast and moist cured for 28 days. The compression test of concrete cubes was performed as per IS 516 (1999). Cylinder of 150 mm diameter and 300 mm height was cast and tested for split tensile strength as per IS 516 (1999). Flexural strength of concrete was measured by testing of beam of 100 mm × 100 mm × 500 mm size under four-point bending using a Digital Universal Testing Machine having a capacity of 60 tons. The results of compression test, split tensile strength and flexural strength of concrete are presented in Table 6.

Table 6. Hardened Properties

Compressive Strength (MPa)	Spilt Tensile Strength (MPa)	Flexural Strength (MPa)
62.64	4.56	4.38

Fracture Test

Fracture test was conducted using a closed loop servo-controlled testing machine under COMD control with the rate of crack opening being 0.0005 mm/s as shown in Figure 3.

The load, CMOD and mid-span vertical displacement acquired during the test are analyzed. Figures 4 and 5 show the load *versus* mid-span vertical displacement and load *versus* CMOD curves,

respectively for small, medium and large specimens. Peak load, displacement at peak load, total displacement, clip gage opening and area under load-displacement curve for all three specimens are presented in Table 7. Results show that peak load, displacement and CMOD increased with increased size of specimen.

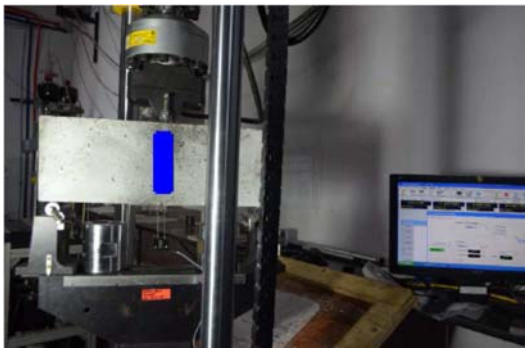

Figure (3): Fracture test set-up and grid pattern used for DIC analysis

Table 7. Peak load, displacement and CMOD

Details	Small	Medium	Large
Peak load (kN)	4.43	6.68	11.70
Displacement at peak load (mm)	0.17	0.43	0.75
Displacement (mm)	0.65	1.21	2.12
CMOD (mm)	1.27	1.72	2.19
Minimum load (kN)	0.03	0.36	0.63
Area under load-displacement curve (kN.mm)	0.53	1.71	5.06

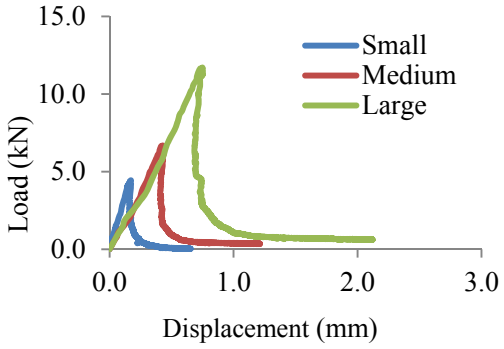

Figure (4): Load *vs.* displacement curve

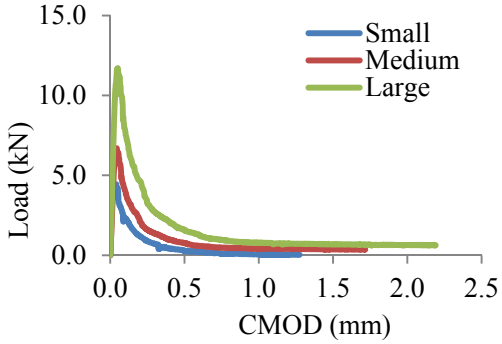

Figure (5): Load *vs.* CMOD curve

The digital images taken during the experiments for all the specimens are correlated using an algorithm originally written by Eberl et al. (2006) using Matlab and modified to suit our requirements. This software uses a normalized cross-correlation algorithm with sub-pixel resolution. The sub-pixel displacement values are obtained through bilinear interpolation between pixels. The algorithm applies a cross-correlation function on two images before and after displacement and identifies the peak. The displacement is assumed to be at the location of the peak of the cross-correlation function. Analysis performed for selected beam is shown in Figure 3. In this figure, the central grid region is superposed on the specimen using image correlation graphics. The displacements are computed in each of x and y directions from within the central grid region. The accuracy of displacement is approximately 0.1 pixel on a point-to-point basis for translational movements. The accuracy of displacement obtained from DIC technique is dependent on the quality of speckle pattern, surrounding vibrations, lighting, out-of-plane displacements and gage length used for strain computations. Hence, it is difficult to give a general guideline for the determination of strain accuracy. The results obtained from the DIC analysis of beams at different stages of loading are presented and discussed in this section.

Displacements

Figure 6 shows a three-dimensional profile of the

deformation taking place during different stages of loading. This figure shows the opening of the crack as the test progresses (depicted by the increasing image number) and is used for quantifying the crack opening displacement which is discussed later on. The results of the vertical displacement at a point close to the notch at the bottom center of the specimen are computed by DIC analysis and measured using an LVDT as shown in Figure 7, together with the vertical load. It is seen that there is a very good match between the vertical displacements computed using DIC and those experimentally measured using an LVDT. This indicates the effectiveness of the DIC technique.

Crack Length

The method employed for determining crack opening displacement (δx), crack tip location and the distance of crack tip (r) from the digitally processed images is shown in Figure 8. The crack tip is located at a point where the crack opening displacement (COD) is zero through visual observation.

The displacements are computed by considering a square grid (zone of interest) in each of x and y directions from within the central grid region. Since the crack tip is located with a precision equal to the size of the correlation window, the crack lengths are resolved to an accuracy of ± 1.25 mm. The crack lengths are computed for all the images and are plotted as shown in Figure 9.

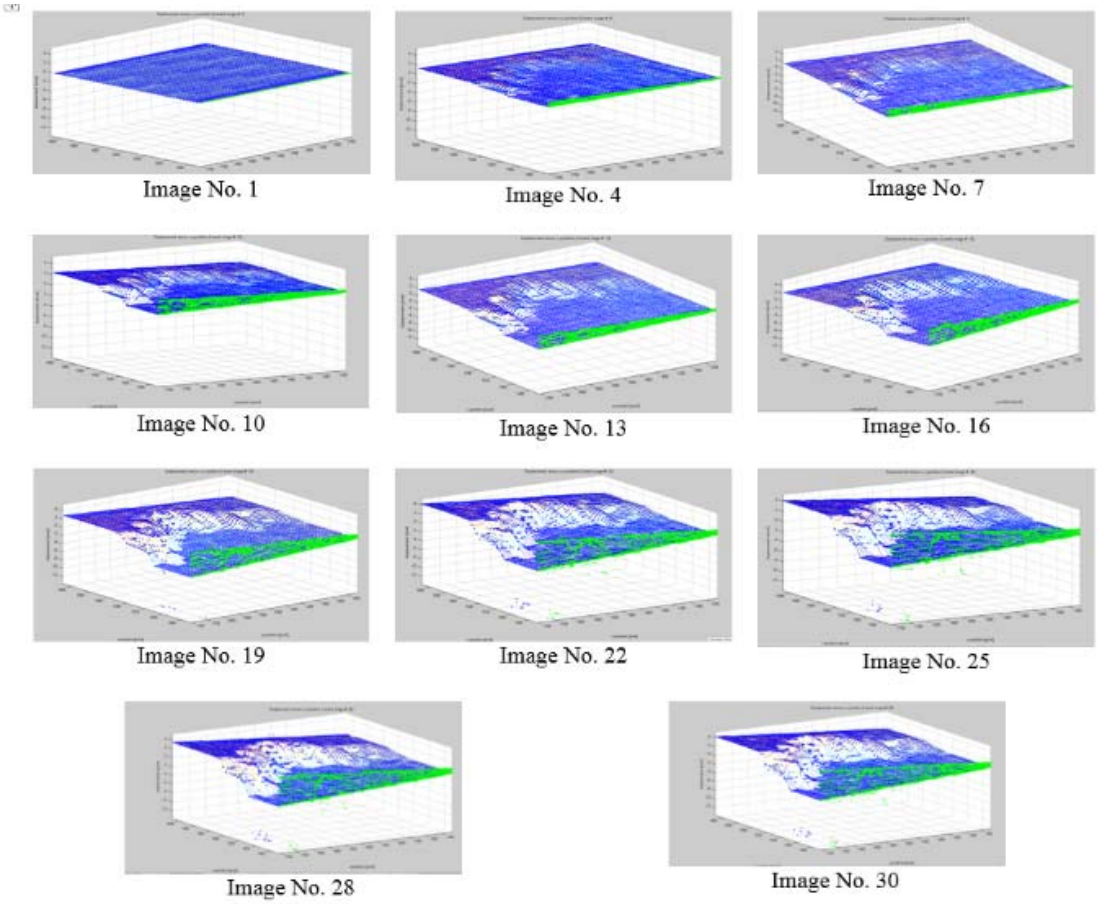

Figure (6): Three-dimensional displacement profile during different stages of loading (medium specimen)

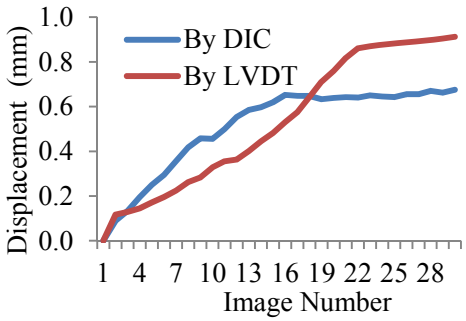

Figure (7): Load *vs.* mid-span vertical displacement (medium specimen)

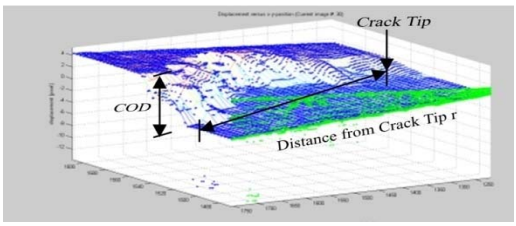

Figure (8): Crack opening displacements and crack length

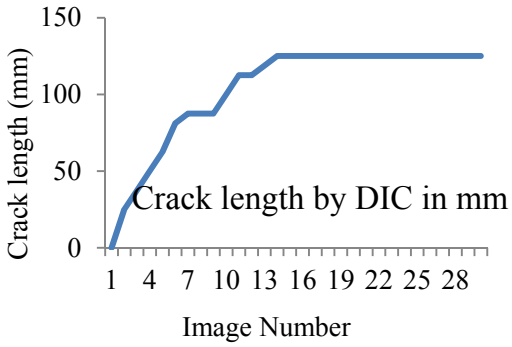

Figure (9): Image number *vs.* crack length

This feature of obtaining the crack tip location and determining of crack length makes the DIC technique very attractive, as it is very difficult to obtain these parameters through other methods. A technique such as dye penetration (Sutton et al., 1986) for determination of crack length has been reported in the literature and is difficult in terms of usage in addition to being expensive.

Crack Mouth Opening Displacement and Crack Sliding Displacement

The advantage of DIC technique is that we can determine the crack opening displacement at any position along the crack, which is not possible with other experimental sensors, such as a clip gage, unless we mount a number of them along the crack. For validation of the results obtained from DIC, the CMOD curves

computed for all the images using DIC analysis are plotted and compared with those experimentally measured using clip gage, as shown in Figure 10. It is seen that there is a very close match between the two. However, one drawback of DIC analysis is that the measurement of CMOD during the initial loading portion is difficult, since the crack does not get initiated as seen from the results of images 1 to 4. While the CMOD gage is fixed at the central position along the thickness of the specimen, the DIC measurements are carried out on the surface. The crack openings are captured by the CMOD gage which does not get transferred onto the surface during the initiation phase of the crack. This may be the possible reason for the above mentioned drawback of the DIC. The accuracy of crack mouth opening and crack sliding displacement is approximately 0.1 pixel.

CONCLUSIONS

The following conclusions are drawn based on the results of the present study.

- As the size of specimen increased, it was observed that there is a delay in load to reach maximum load. It was also observed that the area under load displacement curve increased.
- Good agreement is obtained in vertical displacements and crack mouth opening displacements computed through DIC and those measured using LVDT and clip gage, respectively.
- It can be concluded that simple DIC as an alternative of other techniques can be a very useful and economical substitute against clip gages and LVDTs.

The measurement of crack tip location and crack length can be effectively carried out using DIC techniques, which is very difficult and expensive for concrete-like materials using traditional sensors.

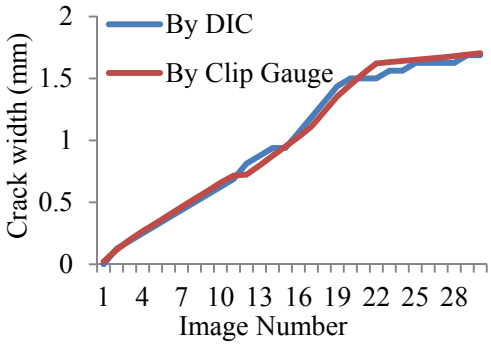

Figure (10): Image number *vs.* crack width

REFERENCES

Bruck, H.A., McNeill, S.R., Sutton M.A., and Peters, W.H. (1989). "Digital image correlation using Newton-Raphson method of partial differential correction". Exp. Mech., 29, 261-267.

Chen, J.L., Zhan, N., Zhang, X.C., and Wang, J.X. (2015). "Improved extended digital image correlation for crack tip deformation measurement". Opt. Laser Eng., 65, 103-109.

Dai, X.J., Yang, F.J., Chen, Z.N., Shao, X.X., and He, XY. (2015). "Strain field estimation based on digital image correlation and radial basis function". Opt. Laser Eng., 65, 64-72.

Debella-Gilo, M., and Kaab, A. (2011). "Sub-pixel precision image matching for measuring surface displacements on mass movements using normalized cross-correlation". Remote Sens. Environ., 115, 130-142.

Eberl, C., Thompson, R., and Gianola, D. (2006). "Digital image correlation and tracking with Matlab". http://www.mathworks.com/matlabcentral/fileexchange/12413.

EFNARC. (2002). "Specification and guidelines for self-compacting concrete". European Association for Producers and Applicators of Specialist Building Products, UK.

Erdem, T.K., Khayat, K., and Yahia, A. (2009), "Correlating rheology of self-consolidating concrete to corresponding concrete-equivalent mortar". ACI Materials Journal, 106 (2), 154160.

Gaimster, R., and Dixon, N. (2003). "Self-compacting concrete Technology". In: Newman, J., and Choo, B.S. (Editors). Advanced Concrete Technology Set. Oxford: Butterworth-Heinemann, 1-23.

Huang, J.Y., Deng, H., Peng, X.L., Li, S.S.., Xiong, C.Y., and Fang, J. (2012). "Cellular traction force reconstruction based on a self-adaptive filtering scheme". Cell Mol. Bioeng., (2), 205-216.

Huang, J.Y., Pan, X.C., Peng, X.L., Zhu, T., Qin, L., Xiong, C.Y., and Fang, J. (2010a). "High-efficiency cell substrate displacement acquisition *via* digital image correlation method using basis functions". Opt. Laser Eng., 48 (11), 1058-1066.

Huang, J.Y., Zhu, T., Pan, X.C., Qin, L., Peng, X.L., Xiong, C.Y., and Fang, J. (2010b). "A high-efficiency digital image correlation method based on a fast recursive scheme". Meas. Sci. Technol., 21, 1-12.

IS 516. (1999). "Methods of tests for strength of concrete". Bureau of Indian Standards, New Delhi.

Lava, P., Cooreman, S., and Debruyne, D. (2010). "Study of systematic errors in strain fields obtained *via* DIC using heterogeneous deformation generated by plastic FEA". Opt. Laser Eng., 48 (4), 457-468.

Najm, H.S. (2008). "Specialized construction applications". In: Nawy, E.G. (Editor). Concrete Construction Engineering Handbook. Boca Raton: CRC Press, 1-26.

RILEM TC 89-FMT. (1990). "Size-effect method for determining fracture energy and process zone size of concrete". Material and Structure, 23, 461-465.

Skarendal, A. (2005). "Changing concrete construction through use of self-compacting concrete". Proceedings of PRO 42-1st International Symposium on Design, Performance and Use of Self-consolidating Concrete SCC'2005. China, 17-24.

Sutton, M.A., Cheng, M., Peters, W.H., Chao, Y.J., and McNeill, S.R. (1986). "Application of an optimized digital correlation method to planar deformation analysis". Image Vis. Comput., 4, 143-150.

Sutton, M.A., Orteu, J.J., and Schreier, H.W. (2009). "Image correlation for shape, motion and deformation measurements". Springer, New York.

Sutton, M.A., Wolters, W.J., Peters, W.H., Ranson, W.F., and McNeill, S.R. (1983). "Determination of displacements using an improved digital correlation method". Image Vis. Comput., 1, 133-139.

Swartz, S.E., and Refai, T. (1989). "Cracked surface revealed by dye and its utility in determining fracture parameters". In: Mihashi H. et al. (Eds.). Fracture Toughness and Fracture Energy: Test Methods for Concrete and Rock. Balkema, Brookfield, 509-520.

Touchal, S.M., Morestin, F., and Brunet, M. (1997). "Various experimental applications of digital image correlation method". Proceedings of International Conference on Computational Methods and Experimental Measurements, Rhodes, Greece, 45–58.

Walter, T.R. (2011). "Low-cost volcano deformation monitoring optical strain measurement and application to Mount St. Helens data". Geophys. J. Int., 186, 699-705.

Wang, X., and Ma, S.P. (2014). "Mesh-based digital image correlation method using non-uniform elements for measuring displacement fields with high gradient". Exp. Mech., 54, 1545-1554.

Wang, Z.Y., Kieu, H., Ngugen, H., and Le, H. (2015). "Digital image correlation in experimental mechanics and image registration in computer vision: similarities, differences and complements". Opt. Laser Eng., 65, 18-27.

Wang, ZZ, Wang, SB, Wang, ZY. (2014). "An analysis on computational load of DIC based on Newton–Raphson scheme". Opt. Laser Eng., 52, 61–65.

Zhang, D.S., and Arola, D.D. (2004). "Applications of digital image correlation to biological tissues". J. Biomed. Opt., 9, 691-699.

Zhang, H., Huang, G.Y., Song, H.P., and Kang, Y.L. (2012). "Experimental investigation of deformation and failure mechanisms in rock under indentation by digital image correlation". Eng. Fract. Mech., 96, 667-675.

Zhou, Y.H., Sun, C., and Chen, J.B. (2014). "Adaptive sub-set offset for systematic error reduction in incremental digital image correlation". Opt. Laser Eng., 55, 5-11.

Zhu, R.H., Xie, H.M., Hu, Z.X., Jiang, L.B., Guo, B.Q., and Li, C.W. (2015). "Performances of different sub-set shapes and control points in sub-set based digital image correlation and their applications in boundary deformation measurement". Appl. Opt., 54 (6), 1290-1301.